Environmental Science Processes & Impacts

ROYAL SOCIETY OF CHEMISTRY

PAPER

View Article Online
View Journal | View Issue

Cite this: *Environ. Sci.: Processes Impacts*, 2023, **25**, 818

A rapid micro chamber method to measure SVOC emission and transport model parameters†

Chunyi Wang,[a] Clara M. A. Eichler,[ab] Chenyang Bi,[a] Christiaan J. E. Delmaar,[c] Ying Xu[d] and John C. Little *[a]

Assessing exposure to semivolatile organic compounds (SVOCs) that are emitted from consumer products and building materials in indoor environments is critical for reducing the associated health risks. Many modeling approaches have been developed for SVOC exposure assessment indoors, including the DustEx webtool. However, the applicability of these tools depends on the availability of model parameters such as the gas-phase concentration at equilibrium with the source material surface, y_0, and the surface–air partition coefficient, K_s, both of which are typically determined in chamber experiments. In this study, we compared two types of chamber design, a macro chamber, which downscaled the dimensions of a room to a smaller size with roughly the same surface-to-volume ratio, and a micro chamber, which minimized the sink-to-source surface area ratio to shorten the time required to reach steady state. The results show that the two chambers with different sink-to-source surface area ratios yield comparable steady-state gas- and surface-phase concentrations for a range of plasticizers, while the micro chamber required significantly shorter times to reach steady state. Using y_0 and K_s measured with the micro chamber, we conducted indoor exposure assessments for di-*n*-butyl phthalate (D*n*BP), di(2-ethylhexyl) phthalate (DEHP) and di(2-ethylhexyl) terephthalate (DEHT) with the updated DustEx webtool. The predicted concentration profiles correspond well with existing measurements and demonstrate the direct applicability of chamber data in exposure assessments.

Received 5th December 2022
Accepted 16th February 2023

DOI: 10.1039/d2em00507g

rsc.li/espi

Environmental significance

Semivolatile organic compounds (SVOCs) including plasticizers can be found in many products, but assessing exposure to SVOCs remains challenging. Exposure modeling tools usually rely on the availability of model parameters measured in chamber experiments, which are generally time-consuming, especially for SVOCs. The micro chamber method presented in this work addresses this issue successfully by reducing the duration of the experiment from days to hours. Furthermore, the comparison of two chambers with different sink-to-source surface area ratios highlights that minimizing the sink-to-source surface area ratio still yields results comparable to those obtained from chambers with more realistic sink-to-source surface area ratios. Thus, model parameters obtained using the rapid micro chamber are applicable in exposure models.

Introduction

Semivolatile organic compounds (SVOCs) are often defined by either their vapor pressure, boiling point, or chromatographic retention time.[1–3] Although the specific ranges given in these definitions may vary slightly,[4] their relatively low vapor pressure leads to SVOCs being present in the indoor environment not only in the gas phase, but also sorbed to airborne particles, settled dust, and indoor surfaces.[5–9] In contrast to volatile organic compounds (VOCs), mass transfer of SVOCs from a source is externally controlled, meaning that the rate limiting step in the emission process is the migration from the source surface to the bulk gas phase.[4,10]

Human exposure to SVOCs in consumer products, articles, and building materials is of great interest because of the large number of SVOCs used for various purposes. Applications of SVOCs range from plasticizers in polyvinyl chloride (PVC) to flame retardants in upholstery and clothing to solvents in paints or pesticides in wood finishes.[11–13] Their ubiquitous presence in indoor environments and the known or suspected toxicity of some SVOCs require a comprehensive understanding of the risk that may be posed by these chemicals.[7,14] The pathways by which people can be exposed to SVOCs indoors then include inhalation of air and airborne particles, ingestion of

[a]*Department of Civil and Environmental Engineering, Virginia Tech, Blacksburg, VA, USA. E-mail: jcl@vt.edu*

[b]*Department of Environmental Sciences and Engineering, University of North Carolina at Chapel Hill, Chapel Hill, NC, USA*

[c]*National Institute for Public Health and the Environment, Center for Safety of Substances and Products, Bilthoven, The Netherlands*

[d]*Department of Building Science, Tsinghua University, Beijing, China*

† Electronic supplementary information (ESI) available. See DOI: https://doi.org/10.1039/d2em00507g

food, ingestion of dust, dermal uptake from air, and dermal uptake by contact with exposed clothing, surfaces or dust, or by contact with a source material.[7,15–17] For SVOCs with relatively low volatility, it has been demonstrated that dust is a major contributor to exposure, especially for toddlers and young children.[18,19] Dust is furthermore of particular interest because it also accelerates SVOC emissions by serving as a sink and thus allowing additional SVOCs to be emitted from a material.[9]

Diisobutyl phthalate (DiBP), di-*n*-butyl phthalate (D*n*BP), di(2-ethylhexyl) phthalate (DEHP), di(2-ethylhexyl)terephthalate (DEHT), and diisononyl phthalate (DiNP) are plasticizers that are very commonly found in indoor air and dust. Because of concerns regarding their adverse health effects, D*n*BP and DEHP have been banned from use in many products for children in the United States (U.S.) since 2008, and DiBP and DiNP have been added to this list in 2017. In Europe, DiBP, D*n*BP, and DEHP are also heavily restricted when used in a variety of products.[14] However, these compounds are still measured with high detection frequencies and concentrations in many indoor samples worldwide.[20–22] At the same time, concentrations of alternative plasticizers like DEHT show an increase in abundance and concentration.[23] This makes exposure assessments for these plasticizers particularly important.

To better predict SVOC emission, transport, and subsequent exposure indoors, modeling approaches have been developed to mechanistically describe SVOC partitioning among the gas-phase, dust, airborne particles, surfaces, and clothing.[9,18,24,25] The publicly available, free DustEx webtool is one example of available tools that incorporate these mechanistic, mass balance-driven modeling approaches to estimate exposure to SVOCs in products that are present in the indoor environment (**https://www.dustex.nl**).[18,24,26] The DustEx tool was developed in 2016 as part of the European Chemical Industry Council's Long-Range Research Initiative (Cefic LRI). It can be used to simulate potential exposures to SVOCs *via* different pathways based on a range of input parameters with a focus on the role of dust in the exposure assessment.[26,27] Extensive documentation of the tool and its underlying equations can be found online.[26] Briefly, the tool is based on SVOC emission and partitioning models developed by Little and Xu (2006),[28] Weschler and Nazaroff (2008)[1] and Weschler and Nazaroff (2012)[29] with the addition of models for exposure evaluation by ingestion of dust and inhalation.[26] The tool is provided online by the Dutch National Institute for Public Health and the Environment (RIVM). However, the applicability of the webtool and other models depends on the availability of critical model parameters, and thus on experimental studies that focus on characterizing emission,[30–33] partitioning,[34–36] indoor conditions,[37–40] and other influencing factors.

Recent findings brought important advances in estimating critical emission and transport parameters necessary for SVOC exposure assessment. These parameters include the SVOC concentration in the gas-phase at equilibrium with the source material surface, y_0, and the surface–air partition coefficient K_s. To successfully predict SVOC emission and transport and resulting human exposure, y_0 is a critical but often unavailable parameter. In general, the SVOC material-phase concentration, C_0, is more readily available. Eichler *et al.* (2018)[41] showed that y_0 can be estimated based on C_0, the saturation vapor pressure p_{sat} and an experimentally derived activity coefficient for plasticizers in PVC products. These findings have been supported in studies by Liang *et al.* (2018)[32] and Addington *et al.* (2020).[42] Liang *et al.*[32] added measurements of organophosphate flame retardants (OPFRs) in rigid foams to the linear relationship found by Eichler *et al.*,[41] thus showing that it can be expanded to other SVOCs and products. K_s on the other hand is used to describe adsorption and desorption of an SVOC to and from a surface that is initially free of the specific SVOC. K_s for clean surfaces depends on the chemical characteristics of the SVOC and on surface properties such as the surface roughness,[34] while for surfaces covered with a thin organic film, K_s can be derived from the octanol–air partition coefficient, K_{oa}.[43] The inclusion of this new knowledge in existing exposure assessment tools such as DustEx is crucial for establishing their validity.

Another challenge for accurate exposure assessment using tools such as DustEx is the lack of experimentally measured emission and transport parameters (y_0 and K_s).[44] Field campaigns and chamber experiments have been conducted to determine those parameters.[45] However, field studies, while having the advantages of obtaining parameters in a real room, are labor-intensive and usually result in high uncertainty in estimated parameters due to poorly constrained environmental conditions (*e.g.*, temperature, air change rate, and the number of sources).[46,47] Additionally, a large number of indoor surfaces in real indoor environments may serve as strong sinks for SVOCs, thus substantially increasing the time needed to reach steady state. On the other hand, chamber experiments, which are typically conducted in well-controlled environments, can measure those critical emissions and transport parameters inexpensively and conveniently, but have to be considered simplified and often idealized representations of real-world scenarios. The sink-to-source surface area ratio in these chambers is usually reduced to shorten the time to reach steady state by orders of magnitude and the surface-to-volume ratio is consequently higher than in a realistic indoor setting, but those chambers no longer represent the dimensions of a real-world room.[48–51] Consequently, there is a critical need to evaluate chamber designs and to demonstrate that chambers with minimized sink-to-source surface area ratios can both represent the characteristics of real indoor environments and be used to conveniently obtain parameters required for exposure assessments. The overarching goal of this study is to close this knowledge gap by comparing different chamber designs to measure SVOC emission and transport parameters and then to use the measured parameters to assess human exposure to SVOCs in real indoor environments with the DustEx webtool. An additional part of this work was to update and validate the DustEx webtool to allow the direct input of parameters obtained from chamber experiments, specifically y_0 and K_s.

Therefore, in this study, we used two types of chambers: a macro chamber, which had a more traditional design in that it downscaled the dimensions of a typical room to a smaller size with roughly the same surface-to-volume ratio as a room, and a micro chamber, which minimized the sink-to-source surface

area ratio to shorten the time until steady state has been reached. The micro chamber is the result of a process of developing chambers aimed at shorter testing times,[32,33,45] which included sandwich-like chambers and material–air–material (M–A–M) chambers, and it is also closely related to the needle trap device microemission cell (NTP-μEC) developed by Xu *et al.* (2019).[51] The specific objectives of this work are to (1) examine whether the two chambers with different sink-to-source surface area ratios can yield comparable results and (2) illustrate the application of the results from the chamber experiments by estimating the concentrations in indoor compartments and human exposure using the updated DustEx webtool.

Materials and methods

Experimental

Chemicals and source materials. Pure dimethyl phthalate (DMP) was used as a liquid emission source for measuring mass-transfer coefficients and obtained from Scientific Polymer Products (Ontario, NY). Standard solutions of DiBP, D*n*BP, DEHP, DEHT, and DiNP, purchased from Sigma Aldrich/Millipore Sigma, St. Louis, MO, were used for chemical calibration and identification. Additional information about the plasticizers, including their CAS RNs and properties, can be found in Table S1 in the ESI.† Deuterium-labeled DEHP (D_4-DEHP) was used as internal standard, and was obtained from AccuStandard (New Haven, CT). Methanol (anhydrous, purity >99%, Sigma-Aldrich) was used as solvent for cleaning and preparing solutions. Dichloromethane (DCM, purity >99.5%, VWR, Radnor, PA) was used for extractions. The solvents were analyzed regularly to monitor for potential contamination.

Two types of vinyl flooring (VF, red and green) and one piece of backpack material were selected as source materials with each material containing several different plasticizers. All three materials have been characterized in previous experiments[31,34,41,52,53] and demonstrated to contain relatively high concentrations of the plasticizers of interest. Their characteristics and the material-phase concentrations of the plasticizers of interest are summarized in Table S2 in the ESI.† Briefly, the VF materials are made of one layer of PVC and the backpack material was made of polyester with a PVC coating.[52,53] Source material pieces were cut into shape for use in either the macro chamber (one rectangular piece, 28 cm by 23 cm) or micro chamber (two round pieces with a diameter of 11 cm). Only red and green vinyl flooring were used in the macro chamber, but all three source materials were tested in the micro chamber.

Macro chamber. The macro chamber consisted of a rectangular box made of type 6063 aluminum and had outside dimensions of 30 cm length by 25 cm width by 13 cm height (Fig. 1a). Aluminum was chosen as the chamber material, because it provides an impervious surface that is easy to clean and to work with, and has been previously characterized in surface partitioning experiments.[34] The air flowed from the inlet, located on one of the short sides of the chamber, passed through the chamber and gas samples were collected from the sampling port at the opposite end of the chamber while extra air was vented through the outlet beside the sampling port. The source material was placed at the bottom of the chamber, covering the bottom entirely, with a source surface area of 6.4×10^{-2} m^2. The surface-to-volume ratio was 37 m^{-1}.

Micro chamber. The micro chamber design is based on the chamber developed by Xu *et al.* (2019),[51] but utilizes a different gas-phase sampling strategy and allows the introduction of rods to study partitioning to different kinds of surfaces. As shown in Fig. 1b, the micro chamber consisted of two round plate covers (bottom and top, 10 cm diameter), and a ring (10 cm outer diameter, 7.6 cm inner diameter, 1.3 cm height). All three parts were made of type 6063 aluminum. Photos of the chambers and a comparison of chamber dimensions are shown in Fig. S1 in

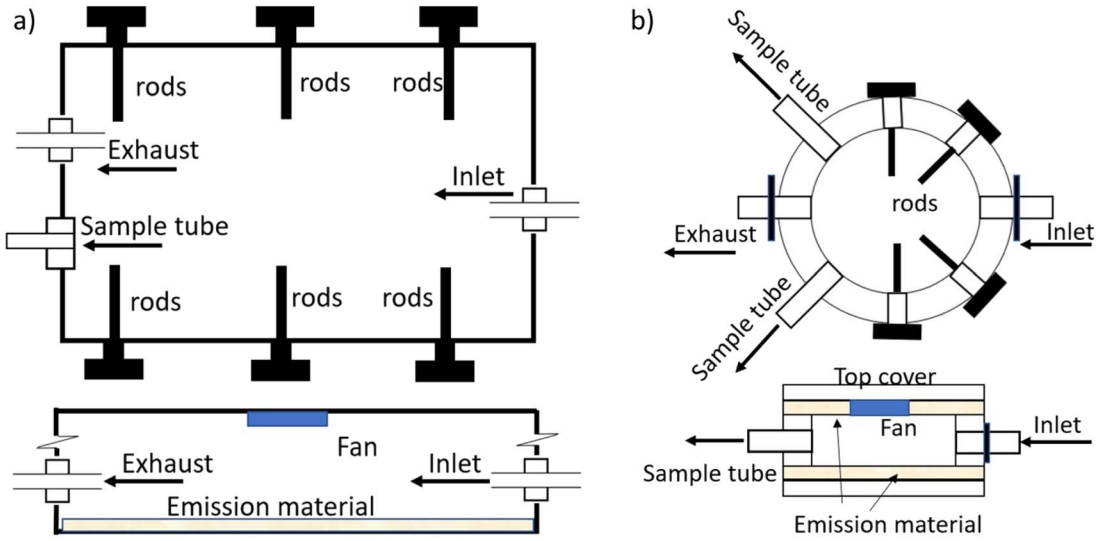

Fig. 1 Schematic top and side view of (a) the macro chamber and (b) the micro chamber. The emission material covers the entire bottom of the macro chamber and the top and bottom of the micro chamber.

the ESI.† Two round pieces of source material were placed between each plate cover and the ring, so that the surface area of the emission source was maximized. Each source material piece had an emission surface area of 4.6×10^{-3} m^2, resulting in a total source surface area of 9.1×10^{-3} m^2. Inlet and outlet lines were aligned 180° to the ring, while two gas-phase sampling ports were located near the outlet. The ring also had four air-tight ports for inserting rods to measure the concentration of plasticizers on the sink surfaces. The resulting surface-to-volume ratio was 12 667 m^{-1}, which is higher than for the macro chamber and much higher than the 1.2 m^{-1} determined for typical rooms without content.[54]

Air tightness of the macro and micro chamber was tested and loss of air was confirmed to be less than 2% by comparing the inlet flow rate with the outlet flow rate with the sampling port sealed. A recirculation fan was attached to the ceilings of both chambers to enhance the mixing of air in the chamber (Fig. S1a and b in the ESI†). All chambers were placed in a temperature-controlled cabinet and operated at 25 ± 0.5 °C. Clean air was provided to the inlet and controlled at 120 and 300 mL min^{-1}, respectively, for the macro chamber and micro chamber, corresponding to an air change rate of 0.96 and 158 per hour. Six (0.31 cm diameter and 5.1 cm length) and four (0.31 cm diameter and 1.3 cm length) aluminum rods attached to a bolt were inserted into the macro and micro chamber, respectively, taken out periodically and analyzed for plasticizers accumulated on the rod the surfaces.

Gas-phase measurements. Gas-phase sampling began immediately after placing the source materials into the chambers. Gas-phase samples of the emitted plasticizers were collected at different time intervals until steady state was reached using thermal desorption (TD) tubes at a constant sampling flow rate of 75 mL min^{-1} for 24 hours. Surplus air passed through the chamber *via* the outlet. The TD tubes were packed with Tenax TA 35/60 (Markes International, Sacramento, CA) as the sorbent. Prior to sampling, the TD tubes were conditioned by heating them to 320 °C for 30 minutes while purging them with nitrogen. Before each experiment, both chambers were cleaned with an alkali detergent, hot tap water, and nanopure water, and then rinsed several times with methanol. After cleaning, gas-phase samples were collected before new source materials were placed into the chamber to monitor plasticizer background levels in the chamber.

Surface-phase measurements. After reaching steady-state gas-phase concentration, aluminum rods were inserted into the chambers and the rods were taken out periodically for SVOC surface concentration analysis to measure the partitioning of analytes from the gas-phase to the surface. Six aluminum rods with a combined surface area of 3.1×10^{-3} m^2 were used with the macro chamber and four aluminum rods with a combined surface area of 5.7×10^{-4} m^2 were inserted into the micro chamber. The rod surface accounts for 1% and 9% of the total sink surface area in the macro and the micro chamber, respectively. Because the rods were made of the same material as the chamber, they provided a means to measure the sorption characteristics of the plasticizers on the chamber surface. Before inserting, the rods were cleaned in an ultrasonic bath with methanol and baked at 300 °C for 30 minutes to ensure that no residuals were left on the surface. After removal from the chamber at predetermined intervals, the rods were quickly placed into clean, empty stainless-steel TD tubes for analysis. The empty TD tubes had been cleaned with methanol, and background concentrations of the tubes were checked before each use. During surface measurements, gas-phase samples were collected periodically to ensure that the gas-phase concentration in the chamber remained at steady state.

Extraction. For extraction of D*n*BP from the "red vinyl flooring" source material, three pieces of flooring were each cut into five smaller pieces of about 1 mm^3 volume and 2 mg weight. The five small pieces of each sample were placed together in flasks containing 25 mL of DCM. To fully dissolve the pieces of flooring, the samples were sonicated for 20 minutes followed by 30 seconds of shaking. This process was repeated three times. For quantification, 1 μL of the extract was injected onto TD tubes and analyzed by TD-GC-FID.

Chemical analysis. All TD tubes, either from gas-phase or surface sampling or spiked with extracts, were desorbed using a thermal desorber (either Markes TD-100 or Turbomatrix 100 TD) and analyzed by either a gas chromatography-mass spectrometry (GC-MS) system (Thermo Scientific DSQII) or a gas chromatography-flame ionization detection (GC-FID) system (Agilent 6890). The GC-MS system was used to analyze samples containing DiNP, since DiNP is a mixture of several compounds with multiple peak signals, and the GC-FID system was used to quantify compounds with a single peak, including DiBP, D*n*BP, DEHT, and DEHP. Before GC-MS analysis, 1 μL solution of D_4-DEHP (20 μg mL^{-1}) in methanol was injected onto each Tenax tube as an internal standard. For GC-FID analysis, the TD tubes were desorbed directly without using an internal standard. Details about the desorption and analytical methods can be found in the ESI.† All tubes were analyzed in two successive runs to ensure complete desorption of the plasticizers from both the TD tube and the TD-GC-MS or -FID system. The second run showed concentrations below the detection limit in all cases.

Modeling

As part of this study, the DustEx tool was updated to allow (1) the estimation of y_0 based on C_0, if the product and the SVOCs meet certain conditions, as described by Eichler *et al.* (2018),[41] and (2) the input of values for K_s for specific sink surfaces, if those are known to the user. Four parameters were measured in the chamber experiments and then used as inputs for the DustEx tool: the plasticizer gas-phase concentration immediately adjacent to the emission source, y_0 (μg m^{-3}), the partition coefficient between the clean surface and the gas-phase, K_s (m), as well as h_m (m h^{-1}) and h_s (m h^{-1}), which are the convective mass-transfer coefficients of the source and sink surface, respectively. The measurements were conducted in two consecutive stages as further described below. Based on chamber measurements, y_0 can be determined using eqn (1):[9,33]

$$y_0 = C_{air,ss} + Q/(h_m S_m) C_{air,ss} \quad (1)$$

where $C_{air,ss}$ (μg m^{-3}) is the SVOC steady-state gas-phase concentration in the chamber, S_m (m^2) is the surface area of the emitting source material, and Q (m^3 h^{-1}) is the air flow rate through the chamber.

To obtain the value of h_m for the target plasticizers, h_m of a reference compound was measured. A more detailed discussion of this procedure can be found in Liang and Xu (2014).[31] Briefly, DMP was chosen as the reference compound since it quickly reaches steady state due to its high volatility. To obtain $h_{m,DMP}$, pure liquid DMP was used as the emission source in the macro chambers instead of a solid source material. In this way, y_0 can be approximated by the vapor pressure of DMP, which leads to a simplification of eqn (1). Then, once $h_{m,DMP}$ is known, h_m of a given plasticizer i can be calculated with eqn (2):[31]

$$h_{m,i}/h_{m,DMP} = (D_{a,i}/D_{a,DMP})^{2/3} = (MW_{DMP}/MW_i)^{1/3} \quad (2)$$

where $D_{a,i}$ and $D_{a,DMP}$ (m^2 s^{-1}) are the diffusion coefficients of plasticizer i and DMP, respectively, in air. MW_{DMP} and MW_i are the molecular weights of DMP and plasticizer i, respectively. It was further assumed that h_s equals h_m for the given chamber conditions.

The sink-surface concentration at steady state, $C_{sur,ss}$ (μg m^{-2}), was then used to derive K_s:[31,34]

$$K_s = C_{sur,ss}/C_{air,ss} \quad (3)$$

The derivations of eqn (1) and (3) are described in detail in the literature.[9,31,34] Unless otherwise stated, all experiment-based calculations and DustEx model predictions presented here were performed in R (RStudio version 3.6.3), using scripts provided by RIVM.

Update of the DustEx tool

Input of measured y_0. By default, DustEx uses the concept of the material–air partition coefficient K_{ma} to relate C_0 to y_0.[26,28] K_{ma} is defined as

$$K_{ma} = C_0/y_0 \quad (4)$$

K_{ma} is a required input in the DustEx tool to relate emission from a source material to the concentration of the compound in the material. C_0 (μg m^{-3}) is a required input for the DustEx tool as well, as 'concentration of the substance in the product'. If y_0 has been measured, K_{ma} can be simply derived by the user using eqn (4) with the appropriate units and input in the tool's interface. If y_0 is not known, the estimation tool described in the following section can now be used.

Implementation of y_0 estimation. In practice, quantitative information on K_{ma} or y_0 for a given material/compound combination is often unavailable. To address this practical limitation, Eichler *et al.* (2018) proposed a predictive relation for y_0, based on measured data for plasticizers in PVC products. The method predicts y_0 from the compound's saturation vapor pressure, p_{sat} (μg m^{-3}):

$$y_0 = \gamma\ w_0\ p_{sat} \quad (5)$$

where γ is an activity coefficient and w_0 is the weight fraction of the compound in the material, which can be determined based on C_0 and the source material density, ρ (g cm^{-3}):

$$w_0 = C_0/\rho \quad (6)$$

With eqn (4)–(6), the relation between K_{ma}, y_0, and C_0 can be transformed to a predictive relation for K_{ma} based on ρ, p_{sat}, and γ:

$$K_{ma} = \rho/(p_{sat}\gamma) \quad (7)$$

The activity coefficient γ was determined to be 5.12 for plasticizers in PVC products.[41] Liang *et al.*[32] determined γ as 3.4 for plasticizers and OPFRs. γ will typically vary between compound groups and material classes.

This estimation method for y_0 was implemented as an input support calculator for the K_{ma} input field. This calculator can be accessed by pressing the 'estimate' button. This brings up an interface to the estimation model. The user should provide vapor pressure, material density, and the activity coefficient. 'Estimate' closes the dialog and fills in the calculated K_{ma} in the input field of the main application. Defaults for the source material density ($\rho = 2$ g cm^{-3}) and for the activity coefficient ($\gamma = 5.12$) are provided but may be overridden by user input.

Extension of K_s specification. The fate of SVOCs in indoor environments is strongly influenced by the transfer of substances to indoor surfaces. DustEx includes a description of this transfer indoors by surface–air partitioning.[26] In the first version of the DustEx tool, surface–air partitioning was conceptualized (following Weschler and Nazaroff[1,24]) as an exchange of SVOC between the air and a thin film of organic material that is assumed to cover all indoor surfaces. In this version of the model, input is required to describe the surface film thickness and the total surface area available for sorption. Partitioning into the surface film is then assumed to be reasonably well approximated by the octanol–air partition coefficient, K_{oa}. Now, in addition to this conceptual description of surface partitioning, an option was added to use measured data of K_s. This is especially appropriate for the simulation of experimental conditions, in which surfaces tend to be clean, and thus are not covered by an organic film as in indoor settings. To use information on the surface/air partition coefficient K_s directly, the mass balance equations in DustEx were modified. The original model equation in the DustEx tool used to calculate the SVOC concentration on the sink surfaces, $C_{sur,v}$ (μg m^{-3}), is

$$dC_{sur,v}/dt = -h_m/d_{sur}(C_{sur,v}/K_{oa} - C_{air}) \quad (8)$$

where d_{sur} (m) is the thickness of the organic film. This equation was rephrased for the case where K_s is used directly:

$$dC_{sur}/dt = -h_m(C_{sur}/K_s - C_{air}) \quad (9)$$

C_{sur} now has the unit of μg m^{-2}. If the user choses to use K_s instead of K_{oa}, the equation to calculate the dynamic change of the gas-phase concentration changes accordingly. The option to

enter a value for K_s was implemented as a radio-button selection. Here, the user may select which sub-model for surface–air partitioning they want to use, either the original, K_{oa}-based 'surface film' option, which requires a specification of the surface film thickness, or the model using input of K_s directly, the 'surface/air partition coefficient' option.

In addition to these changes, ranges of acceptable input values of several DustEx parameters have been expanded to cover a more representative set of indoor and/or experimental conditions. These included the room volume, the ventilation rate, and the dust loading. Expanded ranges have been tested on the aspect of stability of the numerical solver in DustEx by performing repeated Monte-Carlo simulations over the expanded parameter space, testing for proper model integration in the simulated sample. For the exposure assessment, the DustEx webtool version 1.0.2 was used.

Results and discussion

Evaluation and comparison of chamber performances

Fig. 2 shows the gas-phase concentrations of DiBP, D*n*BP, and DEHP measured in the macro chamber and the micro chamber. Table 1 summarizes all resulting measurements. DiBP and D*n*BP (Fig. 2a and b) are comparatively volatile and thus reached their respective steady-state gas-phase concentrations within one day in both chambers (see also Fig. S2 in the ESI† for a close-up of the first 24 hours). The steady-state gas-phase concentrations for each compound were very similar in the two chambers. For DiBP, the steady-state gas-phase concentrations were 171 ± 6.3 μg m^{-3} and 165 ± 6.2 μg m^{-3} in the macro and the micro chamber, respectively. The D*n*BP steady-state gas-phase concentrations were 69 ± 2.2 μg m^{-3} and 73 ± 3.5 μg m^{-3} in the macro and micro chamber, respectively. However, the gas-phase concentration of DEHP, whose vapor pressure is two orders of magnitude lower, did not reach steady state over the course of 40 days in the macro chamber. In the micro chamber, the steady-state gas-phase concentration of DEHP, 2.3 ± 0.2 μg m^{-3}, was reached after about 6 days. The shortened time to reach equilibrium for less volatile compounds indicates a clear advantage of the micro chamber. Based on the $C_{air,ss}$ values for DiBP, D*n*BP, and DEHP, y_0 was calculated for the different source materials as described in eqn (1). The results show that for DiBP and D*n*BP, the two chambers yielded comparable results, but for DEHP, the macro chamber could not be used to assess y_0 within a reasonable time frame.

The surface concentrations of DiBP and D*n*BP on the aluminum rods inserted into the macro and the micro chamber are shown in Fig. 3. Surface measurements in the macro chamber were only conducted with DiBP and D*n*BP. As with the gas-phase concentrations, the surface concentration profiles measured in both chambers are similar, however, for both phthalates, the macro chamber yielded slightly higher steady-state surface concentrations. Differences in the air change rate and the mixing conditions in the chambers are possible reasons for the discrepancy, because they may result in boundary layers with different thicknesses and thus varying surface concentrations on the rods. Data from both chambers

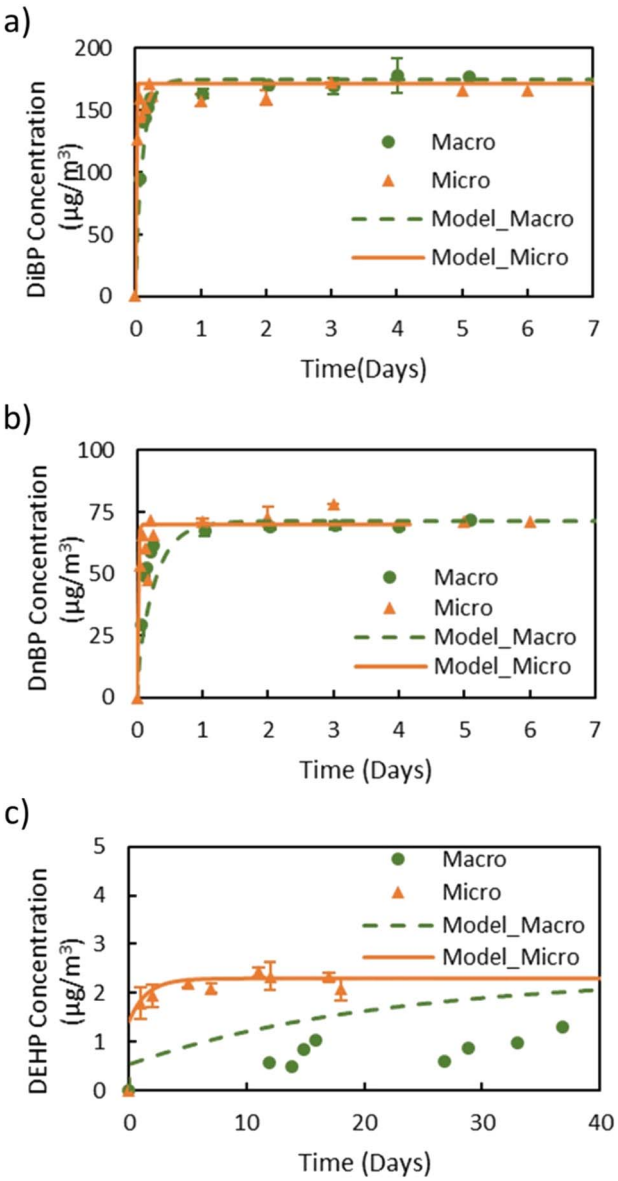

Fig. 2 Comparison of the gas-phase concentrations of selected plasticizers over time in the macro chamber and in the micro chamber for (a) DiBP, (b) D*n*BP, and (c) DEHP. Dots and triangles refer to measured gas-phase concentrations in the macro and micro chamber, respectively, while the lines are DustEx model predictions.

were used to determine K_s of DiBP and D*n*BP as described in eqn (3) and resulted in very comparable K_s values (Table 1). Fig. S3 in the ESI† further illustrates that the surface concentrations were independent of the location of the rods in the micro chamber.

In addition to the experimental results, the gas-phase concentration profiles of DiBP, D*n*BP, and DEHP in the macro and micro chambers as well as the surface concentrations profiles of DiBP and D*n*BP were predicted with the DustEx model (Fig. 2 and 3), using y_0, K_s and h_m derived directly from the chamber experiments (Table 1) as well as additional input parameters like chamber volume and air change rate in the

Table 1 Parameters obtained from the chamber experiments

	Macro chamber			Micro chamber				
Plasticizer	DiBP	D*n*BP	DEHP	DiBP	D*n*BP	DEHP	DEHT	DiNP
Steady-state gas-phase concentration $C_{air,ss}$ (μg m^{-3})	171 ± 6.3	69 ± 2.2	1.3[a]	165 ± 6.2	73 ± 3.5	2.3 ± 0.2	0.50 ± 0.02	0.12 ± 0.01
Steady-state surface concentration $C_{sur,ss}$ (μg m^{-2})	1795 ± 100	1608 ± 81	NA[a]	1305 ± 40	1295 ± 30	3242 ± 341	898 ± 77	222 ± 18
Mass-transfer coefficient of the source surface h_m[c] (m h^{-1})	13	13	12	73	73	65	65	63
Gas-phase concentration immediately adjacent to the emission source y_0 (μg m^{-3})	172	69.6	NA[a]	169	75.0	2.37	0.515	0.124
Surface–air partition coefficient for aluminum K_s (m)	10 ± 0.7	23 ± 1.7	NA[a]	8 ± 1.1	18 ± 2.1	1410 ± 26	1800 ± 82	1850 ± 5
Material-phase concentration C_0[b] (wt%)	4.6	3.8	23.3	4.6	3.8	23.3	7.9	4.2

[a] Steady state had not been reached during the course of the experiment. [b] Measured in previous studies.[52,53] See Table S2. [c] h_m is calculated with eqn (2) using pure liquid DMP as emission source.

chamber (Table S4†). Overall, the model predicts the measured concentrations very accurately for both chambers, especially the gas-phase and surface concentrations at steady state, which gives confidence in the model's overall performance. For predicting the surface concentrations, the model assumes that $h_{s,DiBP} = h_{m,DiBP} = 13$ m h^{-1}, as calculated based on the measured value of $h_{m,DMP} = 14.6$ m h^{-1} and eqn (2) in macro chamber. The results show that DiBP and D*n*BP have the same h_m. However, the model seems to slightly underpredict the surface concentration before steady state has been reached, and thus overpredicts the time needed for steady-state conditions to be achieved (Fig. S4 in the ESI†). The most likely reason for this difference is the assumption that h_s and h_m are equal. When fitting the model directly to the experimental data, more accurate values for h_s can be obtained: 43 m h^{-1} and 35 m h^{-1} for DiBP and D*n*BP, respectively. These fitted h_s values are still on the same order of magnitude as h_m, and because the choice of h_s (assumed or fitted) has no significant influence on the predicted steady-state surface concentrations, we used the assumption of $h_s = h_m$ for all further calculations and model predictions.

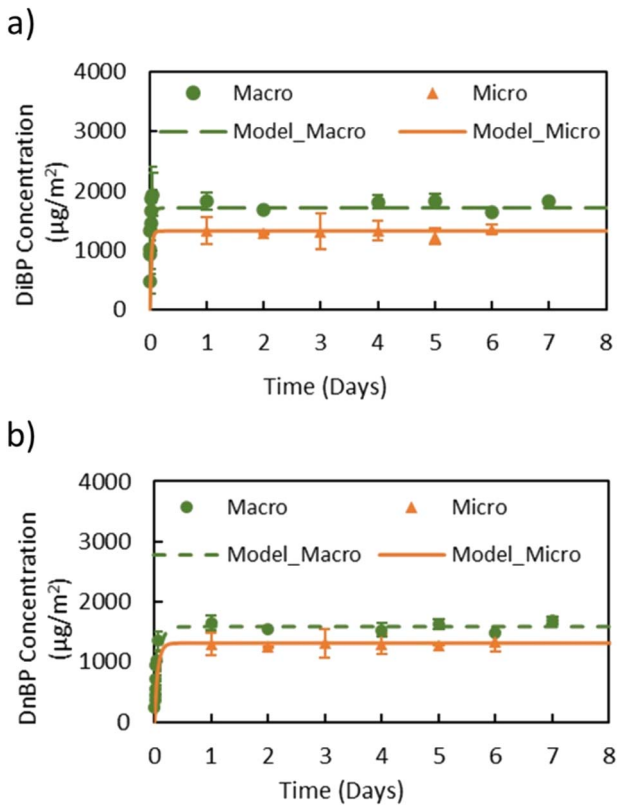

Fig. 3 Comparison of the surface-phase concentrations of (a) DiBP and (b) D*n*BP on aluminum rod surfaces in the macro chamber and micro chamber. Dots and triangles refer to measured surface-phase concentrations in the macro and the micro chamber, respectively, and the lines represent DustEx model predictions.

Although the macro chamber and the micro chamber are significantly different in their dimensions and configurations, their gas-phase concentrations of DiBP and D*n*BP agreed well and the concentrations on the rod surfaces were comparable. A major reason for the agreement of gas- and surface-phase concentrations is that the values of the mass-transfer coefficients in both the macro and micro chamber are high due to the installation of the recirculation fan. In fact, the h_m values of the plasticizers included in this study (12–73 m h^{-1}) are two orders of magnitude higher than those in previous chamber studies.[33,48,55] Consequently, the term $Q/h_m/S_m$ in eqn (1) becomes small and even negligible, meaning that $C_{air,ss} \approx y_0$. In this case, the measured gas-phase concentration in the chamber, $C_{air,ss}$, is mathematically independent of chamber dimensions and flow rate. Therefore, by substantially increasing the mass-transfer coefficients in the chamber, the approach allows the determination of y_0 directly using only the steady-state gas-phase concentration in the chamber. Such an approach may avoid using other parameters including h_m, which may vary significantly depending on the physical

property of the analyte and surface airflow conditions that are difficult to determine experimentally.

In general, the main difference between the chambers is the time needed for the plasticizers emitted from the source material to reach steady state in the gas-phase of the chamber. Due to the high ratio of sink-to-source surface area in the macro chamber, it takes a much longer time for low-volatility compounds like DEHP to reach steady state. Therefore, the micro chamber was selected for performing the remaining experiments, *i.e.*, for measuring y_0 of a source material containing DEHT and DiNP and for measuring K_s of these two plasticizers. The gas-phase concentration profiles for DEHT and DiNP are shown in Fig. 4, the surface concentration profiles can be found in Fig. 5, and the results are also summarized in Table 1. As expected, the time required to reach steady state increases further for those low-volatility compounds, even with the micro chamber, but is still reasonable at 8–10 days. It can be observed that the steady-state gas-phase concentrations correlate with the volatility of the plasticizers, *i.e.*, they decrease with decreasing vapor pressure. This matches observations from other studies.[46,56] On the other hand, the surface–air partition coefficient increases with decreasing vapor pressure, resulting in higher surface concentrations relative to the gas-phase concentrations for low-volatility compounds. However, as can be seen for DEHP, which has the highest material-phase concentration, the steady-state concentrations also depend on how much plasticizer was initially present in the source material. Thus, DEHP has the highest steady-state surface concentration, despite its higher vapor pressure compared to DEHT and DiNP.

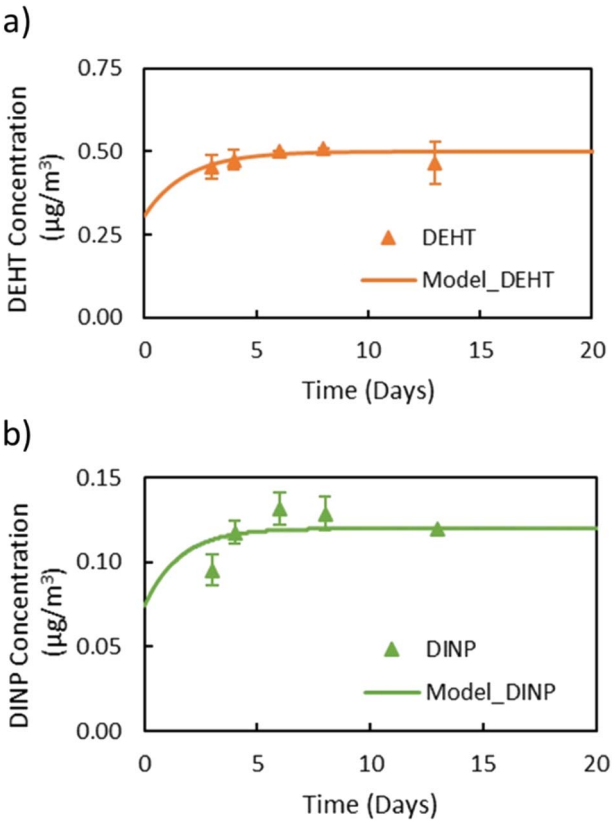

Fig. 4 Gas-phase concentrations of (a) DEHT and (b) DiNP over time in the micro chamber. Dots refer to measured gas-phase concentrations and the lines are DustEx model predictions.

Previously, y_0 of the source materials used in this study had been determined using small diffusion chambers.[31,41,52] In these studies, y_0 of DEHP in the green VF source material was measured to be 2.4 μg m^{-3} and y_0 of DEHT and DiNP in the backpack source material were 0.8 μg m^{-3} and 0.1 μg m^{-3}, respectively, which is very close to the results for y_0 in this study. In Eichler *et al.* (2018),[41] the measured y_0 value was excluded from the data set because it exceeded the vapor pressure of 0.4 μg m^{-3}. Here, y_0 of DEHT is slightly lower, but still higher than the vapor pressure. Further, the y_0 values measured in this study with the micro chamber for D*n*BP and DiBP in the red VF source material, 75.0 μg m^{-3} and 169 μg m^{-3}, respectively, are significantly higher than those reported in previous studies for the same material. Wu *et al.* (2015)[52] determined y_0 of D*n*BP and DiBP of this material to be 25 μg m^{-3} and 49.8 μg m^{-3}, respectively, while Cao *et al.* (2016)[57] reported 36 μg m^{-3} and 68 μg m^{-3}. To address the possibility of a change of the material-phase concentration (C_0) over time, the VF source material was extracted using the same method reported by Wu *et al.* (2015).[52] The extraction showed that the material has a DiBP and D*n*BP weight fractions of 4.6% and 3.5%, respectively, which are close to the weight fraction of 4.6% and 3.8% measured by Wu *et al.* (2015)[52] and thus unlikely to explain the elevated y_0 values. In contrast to the increase in y_0 of D*n*BP and DiBP in this study compared to previous studies, y_0 of DEHP measured in this study still agrees with earlier measurements.[52,57] Further investigation is needed to better understand the reasons for the increase in y_0 of D*n*BP and DiBP in this material.

Wu *et al.* (2017)[34] investigated the partitioning of DEHP to different types of impervious surfaces, including DEHP. Based on their study, K_s of DEHP for aluminum surfaces is 600 m, which is almost 2.5 times smaller than the K_s value measured in this study (1410 m). The most likely reason is that a different type of aluminum was used here with a slightly higher surface roughness, which would have led to an increase in K_s. Another possible reason for the discrepancy is the different analytical methods used in the two studies. Wu *et al.* (2017) extracted the adsorbed DEHP from the surface, while in this study, the rods were directly thermally desorbed, which could have resulted in reduced loss during sample preparation and thus would have increased K_s. Altogether, the results are still similar enough to give overall confidence in the micro chamber method.

Predicting plasticizer concentrations in a simulated room

The comparison of the measured data from the chamber experiments with the concentration profiles predicted by the DustEx model shows overall very good agreement. However, the DustEx tool is mainly intended to provide exposure information for real indoor environments. Thus, we used the information obtained from the micro chamber experiments to predict the

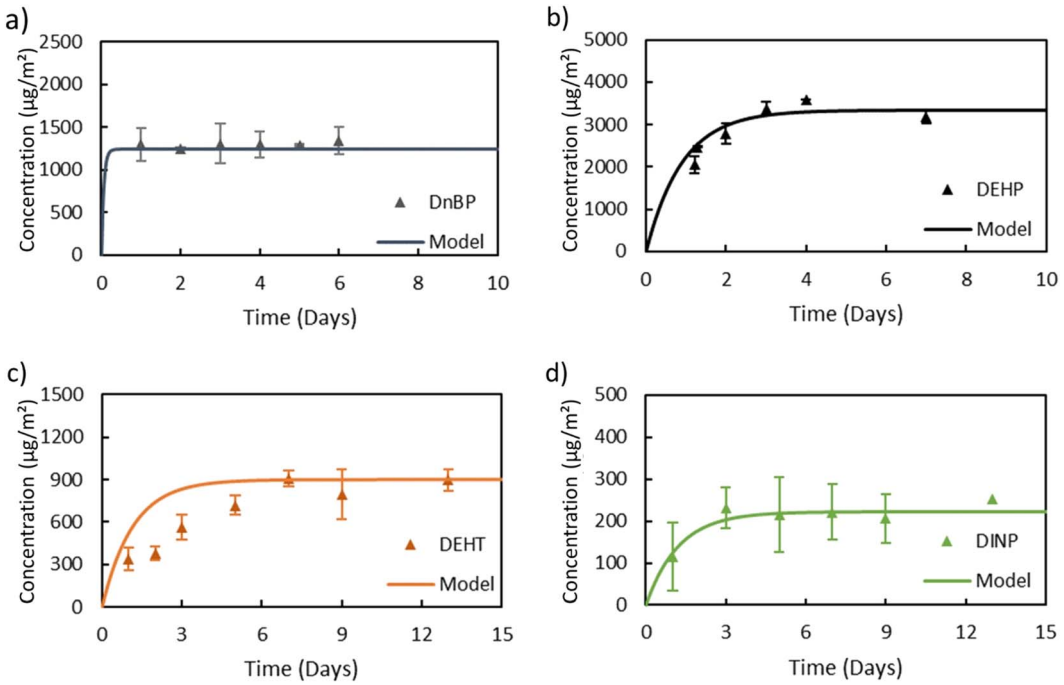

Fig. 5 Comparison of the surface concentrations of (a) D*n*BP, (b) DEHP, (c) DEHT, and (d) DiNP on aluminum rod surfaces in the micro chamber. Dots refer to measured concentrations on the rods and lines are DustEx model predictions.

concentrations of D*n*BP, DEHP and DEHT in a room with the updated DustEx tool. These three plasticizers were selected because D*n*BP and DEHP are commonly found indoors, but have different volatilities, and DEHT is a common substitute for DEHP. The room was defined to have a volume of 50 m^3 and an air change rate (λ) of 0.5 h^{-1}. This air change rate corresponds to the geometric mean derived from multiple studies in a recent review by Nazaroff (2021).[58] It was further assumed that the source surface area in the room is 20 m^2 (*i.e.*, the floor) and the sink surface area is 160 m^2, based on a surface area-to-volume ratio with room contents of 3.2 m^{-1}, as determined by Manuja *et al.* (2019).[54] The y_0 and K_s values obtained from the chamber experiments for D*n*BP, DEHP and DEHT were used in the model, assuming the same source material as the emission source in the chambers (vinyl flooring) and sink surfaces consisting of aluminum (see Table S5† for model input parameters). It was assumed that no additional sources of the respective plasticizer exist in the room. For model parameters that are not directly related to the room or the compounds, default values of the DustEx tool were used (Table S5†).

Fig. 6 shows a comparison of the resulting concentrations in different indoor compartments for D*n*BP and DEHP, as predicted by the DustEx tool for a 30 day simulation. Results for all three plasticizers for a 365 day simulation period can be found in the ESI (Table S6 and Fig. S5–S7†). After 30 days, the concentrations of D*n*BP in all indoor compartments have reached steady state, however, for DEHP, the concentrations of DEHP in the compartments that depend on partitioning (particles, dust, and surfaces), have not yet reached steady state. The gas-phase concentration of DEHP also takes significantly longer than the gas-phase concentration of D*n*BP to reach steady state. A comparison of the DEHP concentrations in the four indoor compartments after 365 days of simulation with the concentrations after 730 days (2 years) shows that the steady state has also not been reached after 1 year. These differences in the behavior show clearly the effect that their respective properties, especially their different vapor pressures and resulting partitioning behavior, have on SVOC distribution indoors. A comparison with DEHT highlights that DEHP and DEHT behave very similarly, and the lower DEHT concentrations in the indoor compartments after 365 days can be attributed to the lower concentration of DEHT in the source material compared to DEHP. Additionally, Fig. S8 in the ESI† shows a comparison between the gas-phase concentration profiles of DEHP in the micro chamber and in the room. It can be seen that it takes a significantly longer time for the gas-phase concentrations in the simulated room to reach steady state. In addition, the steady-state concentrations are always lower in the room compared to the chamber, due to the larger volume and increased sink surface area in relation to the source surface area. The comparison further illustrates the different time scales at which the chamber and a realistic indoor environment operate.

D*n*BP associated with airborne particles plays a minor role in the concentration profile compared to DEHP and DEHT, which have both a larger particle-bound fraction than gas-phase fraction. For all three compounds, the surface is an important sink, followed by dust. However, the role of dust is of greater relative importance for D*n*BP than for DEHP and DEHT, likely driven by the two order of magnitude lower K_s of D*n*BP. In addition, all surfaces were considered to be aluminum, which is an unrealistic assumption, but helps describing surface sinks and

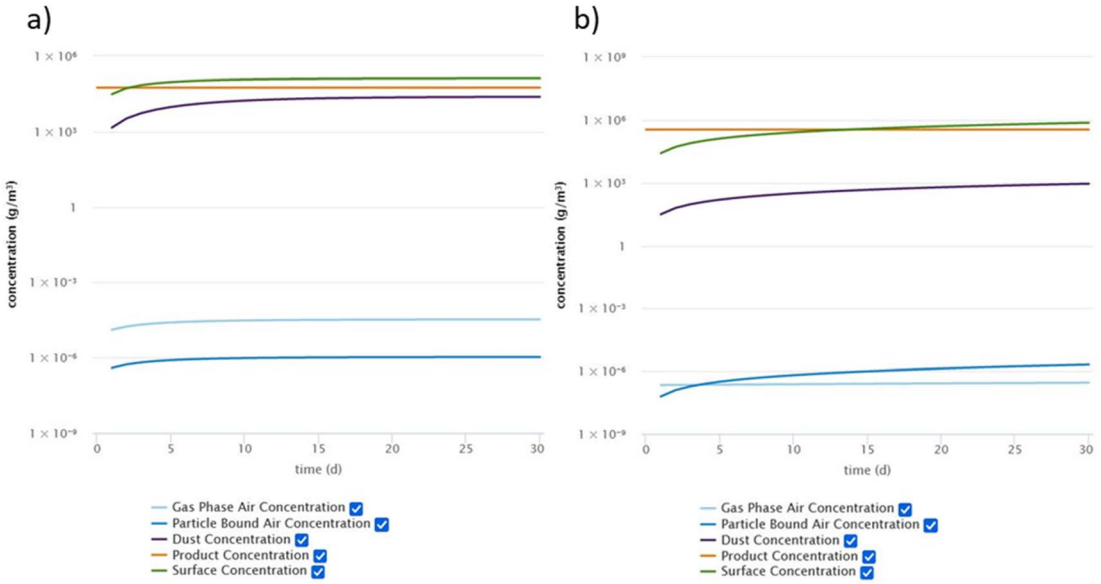

Fig. 6 Concentrations of (a) D*n*BP and (b) DEHP in indoor compartments as calculated by the DustEx tool over 30 days.

illustrates the large potential of indoor surfaces to accumulate SVOCs and to become reservoirs.[6] Overall, the predicted concentrations of the three plasticizers in the gas phase, particle phase and dust follow the trends of existing measurements. Huang *et al.* (2021)[22] measured D*n*BP and DEHP in these three compartments in homes in South China and observed similar distributions, with D*n*BP present at a much higher fraction in the gas phase than in the particle phase compared to DEHP, and with both phthalates being present at high concentrations in the dust. The measured DEHP concentration in dust was 3.6×10^5 ng g^{-1} dust, compared to 3.2×10^6 ng g^{-1} predicted by the DustEx tool (converted from Table S6† assuming a dust density of 2 g cm^{-3}). Hammel *et al.* (2019)[59] measured D*n*BP, DEHP and DEHT in dust from homes in North Carolina and found median concentrations of DEHP and DEHT within one order of magnitude of the DustEx predicted concentrations. Similar results were found for DEHP and DEHT by Tang *et al.* (2020)[60] for dust from bedrooms and offices in Guangzhou, China and by Nagorka *et al.* (2022)[23] for house dust from Germany. The D*n*BP concentrations in dust reported in both studies are within three orders of magnitude of each other.[23,60] However, measured results for D*n*BP tend to be generally lower than the DustEx prediction. Also, measured gas-phase and particle-phase concentrations of all three plasticizers tend to be lower than predicted, although measurements by Huang *et al.* (2022)[61] of D*n*BP in indoor air and PM2.5 in homes in Beijing are comparable to those predicted by the DustEx tool. The choice of K_s value influences the resulting concentrations in air. Many indoor surfaces have likely a much higher K_s than that for aluminum, which would result in lower air concentrations and even greater accumulation on surfaces and in porous materials. Some of the observed differences can also be attributed to the highly simplified conditions assumed in the model and the unlikely assumption that equilibrium conditions are achieved in the way the DustEx tool estimates them. Therefore, the selection of higher K_s values, shorter simulation durations and the introduction of more disturbances may result in more comparable results.

Overall, our observations confirm that the DustEx model accurately predicts general trends observed in real indoor environments based on chemical properties and measurements obtained from chamber experiments, which in turn have implications for exposure assessments. The results further suggest that K_s values are very important parameters for the prediction of gas-phase concentrations in homes, especially for describing the influence of porous surface materials, which may behave as strong sinks and thus strongly influence dynamic air concentrations. Despite simplified and conservative settings for the simulation, the estimated concentrations for the gas phase, particle phase and dust are comparable with some existing measurements, but exceed others.[20]

Exposure assessment with the DustEx tool

The updated DustEx tool also yields predictions of subsequent exposures to D*n*BP, DEHP and DEHT for a child and an adult in the room described before. Table S7 in the ESI† summarizes the resulting absorbed doses and Fig. S9–S11† shows the absorbed dose of each plasticizer by absorption pathway over time. The exposure assessment illustrates that the absorbed doses of D*n*BP quickly reach their steady state (Fig. S9†), in accordance with the observations for D*n*BP in indoor compartments. For DEHP and DEHT, it takes more than 1 year to achieve constant daily absorption doses (Fig. S10 and S11†). For children, DEHP and DEHT exposure is dominated by the ingestion of dust, while for D*n*BP dermal absorption from the air plays a much greater role, followed closely by dust ingestion. For adults, the role of dermal absorption of D*n*BP is much greater than for children, as is the inhalation of particle-bound DEHP and DEHT. This corresponds to high DEHP and DEHT

concentrations in the dust and bound to particles (Tables S6 and S7†). Because of the importance of dust ingestion for DEHP and DEHT exposure, children's exposure to these compounds is actually slightly higher than for adults. However, because dermal uptake from the gas phase is higher for adults, children have an overall lower exposure to D*n*BP. Further, based on the model prediction, the highest plasticizer concentrations are associated with surfaces. The DustEx tool does not include exposure by contact to contaminated surfaces; instead, these surfaces are incorporated as sinks. Here, potential for further expansion of the model can be seen.

These results highlights the direct applicability of the parameters obtained from the chamber experiments for exposure assessments. For example, the estimated exposures can be compared to reference values, such as the Tolerable Daily Intake (TDI) set by the European Food Safety Authority (EFSA) or the Minimal Risk Levels (MRLs) established by the U.S. Agency for Toxic Substances and Disease Registry (ATSDR). The EFSA TDI set for D*n*BP, DEHP and DiNP, which is a group TDI that also includes butylbenzyl phthalate (BBzP), is 50 μg per kg BW per d.[62] The results obtained from the DustEx tool show that the absorbed dose of D*n*BP for children and adults under the given conditions is actually above the EFSA TDI and thus potentially of concern. The acute oral MRL for D*n*BP is 500 μg per kg BW per d and for DEHP is 3.0 μg per kg BW per d.[63] For DEHP, this is clearly exceeded by the exposure of a child to DEHP in dust and also for adults by inhalation of particle-phase DEHP, indicating a potential high-risk scenario. The exposure results obtained from the DustEx tool could further be linked to physiologically-based pharmacokinetic (PBPK) modeling approaches to predict body burden and compare with *in vitro* toxicity data for further risk management and chemical prioritization, as demonstrated by Wu *et al.* (2021).[64] However, as discussed above, these exposure estimates have to be evaluated within the limitations of the tool and its parameters.

Limitations and future work

Only a small range of plasticizers was studied using previously characterized source materials. Because experiments using the micro chamber were shown to be time-efficient and reproducible, future work should focus on applying this method to measure critical model parameters for a broader range of SVOCs. In addition, the micro chamber can be used to better understand specific factors that influence emissions, such as the composition of the source material, different levels of SVOCs in the source material, and temperature. The only limitation for the use of the micro chamber at this point is that the source material has to be flat. Further, only one type of sink material, aluminum, was used in this study to obtain K_s. However, other sink materials could be easily introduced into the chamber as rods, including glass, wood, or laminated surfaces. The chamber also allows the study of variations in surface characteristics, such as surface roughness, by introducing rods with different properties. For some surfaces, direct thermal desorption of the rods may not be possible, so that extraction methods would have to be developed. The DustEx tool will have to be updated regularly in the future to include recent findings and model improvements. Additional options that allow the choice of specific indoor environmental compartments to be included and for a broader range of SVOCs to be assessed with the tool would also broaden its user-friendliness and applicability.

The DustEx webtool and its underlying models were used to predict plasticizer concentrations in indoor compartments and resulting exposures. However, the model has several simplifications and is based on the assumption of equilibrium between the compartments, which is not always true in real indoor environments, especially for low-volatility SVOCs like DEHP. Currently, the DustEx tool is limited to the input of SVOCs with a $\log(K_{oa})$ in the range of 7 to 13, which excludes SVOCs that are very unlikely to reach equilibrium, like DiNP. Further, comparing predicted doses with existing measurements was beyond the scope of this study, but such an assessment of the results is strongly recommended to users of the DustEx tool and other exposure modeling tools. It should also be noted that for the exposure assessment, default values of the DustEx tool were used, which can be considered reasonable, but are also rather conservative and not applicable to all situations.

Conclusions

In this study, we compared two types of chamber design for measuring the gas-phase concentration of SVOCs at equilibrium with the source material surface, y_0, and the surface–air partition coefficient, K_s: a macro chamber, which downscaled the dimension of a room to a smaller size with roughly the same surface-to-volume ratio, and a micro chamber, which minimized the sink-to-source surface area ratio to shorten the time required to reach steady state. Here, the focus was on emission and partitioning of commonly found plasticizers in PVC source materials. The results showed that the two chambers with different sink-to-source surface area ratios yield comparable steady-state gas- and surface-phase concentrations of SVOCs while the micro chamber required a significantly shorter time to reach steady state. The close agreement of steady state concentrations between the two chambers was caused by the enhancement of mass transfer coefficient, h_m, through the installation of the mixing fan. The micro chamber used in this study could potentially allow the determination of y_0 directly using only the steady-state gas-phase concentration in the chamber. Such an approach may avoid using other parameters, including h_m, which may vary significantly depending on the physical properties of the analyte and surface airflow conditions that are difficult to determine experimentally. Overall, the micro chamber shows significant advantages compared to other chamber designs, such as the minimized sink-to-source surface area ratio to shorten the time required to reach steady state and the increased mass-transfer coefficient to make the gas-phase concentration independent of chamber dimensions and flow rate.

The DustEx webtool was updated as part of this study to allow the direct input of chamber measurements of y_0 and K_s. This functionality further broadens the tool's applicability to

predict human exposure to SVOCs in indoor environments. We illustrated how the resulting parameters can be applied to predict concentrations of different plasticizers in indoor compartments as well as human exposure indoors. The results showed that the predicted and measured concentrations agree generally well, but also that resulting exposure estimates have to be evaluated in the context of the parameters chosen for the simulation. In combination, the micro chamber and the DustEx model provide means for high-throughput exposure estimates and can be potentially applied for rapid, screening level risk assessments.

Author contributions

CW conducted the experimental work, performed data analysis and interpretation, and contributed to the manuscript. CMAE wrote the manuscript and contributed to the experimental work, data analysis, and data interpretation. CB contributed to the experimental work, data analysis and interpretation, and manuscript revision. CJED updated the DustEx model and contributed to the manuscript. YX contributed to the micro chamber development and data interpretation. JCL contributed to all aspects of the research and manuscript preparation, and devised and supported the research.

Conflicts of interest

The authors declare no conflict of interest.

Acknowledgements

Support for this research was provided by the Long-Range Research Initiative (LRI) of the European Chemical Industry Council (Cefic), project code LRI-B12.3. The authors thank Rainer Otter and the Cefic-LRI monitoring team for valuable input.

References

1 C. J. Weschler and W. W. Nazaroff, Semivolatile organic compounds in indoor environments, *Atmos. Environ.*, 2008, **42**(40), 9018–9040.
2 WHO, *Indoor Air Quality: Organic Pollutants*, World Health Organization, Copenhagen, NL, 1989.
3 ISO, ISO 16000-6 Indoor air – Part 6: Determination of volatile organic compounds in indoor and test chamber air by active sampling on Tenax TA sorbent, thermal desorption and gas chromatography using MS or MS-FID, in *13.040.20 - Ambient Atmospheres*, International Organization for Standardization, 2021, p. 36.
4 ASTM, Standard Guide for Selecting Volatile Organic Compounds (VOCs) and Semi-Volatile Organic Compounds (SVOCs) Emission Testing Methods to Determine Emission Parameters for Modeling of Indoor Environments, in *ASTM International*, 2022, vol. ASTM D8141-22, p. 11.
5 J. Cao, Semi-volatile Organic Compounds (SVOCs), in *Handbook of Indoor Air Quality*, ed. Zhang, Y., Hopke, P. K. and Mandin, C., Springer Nature, Singapore, 2022, pp. 99–127.
6 NASEM, *Why Indoor Chemistry Matters*, National Academies of Sciences, Engineering, and Medicine, Washington, DC, 2022, p. 176.
7 C. M. A. Eichler, E. A. Cohen Hubal, Y. Xu, J. Cao, C. Bi, C. J. Weschler, T. Salthammer, G. C. Morrison, A. J. Koivisto, Y. Zhang, C. Mandin, W. Wei, P. Blondeau, D. Poppendieck, X. Liu, C. J. E. Delmaar, P. Fantke, O. Jolliet, H.-M. Shin, M. L. Diamond, M. Shiraiwa, A. Zuend, P. K. Hopke, N. von Goetz, M. Kulmala and J. C. Little, Assessing Human Exposure to SVOCs in Materials, Products and Articles: A Modular Mechanistic Framework, *Environ. Sci. Technol.*, 2021, **55**(1), 25–43.
8 D. Licina, G. C. Morrison, G. Bekö, C. J. Weschler and W. W. Nazaroff, Clothing-Mediated Exposures to Chemicals and Particles, *Environ. Sci. Technol.*, 2019, **53**(10), 5559–5575.
9 J. C. Little, C. J. Weschler, W. W. Nazaroff, Z. Liu and E. A. Cohen Hubal, Rapid Methods to Estimate Potential Exposure to Semivolatile Organic Compounds in the Indoor Environment, *Environ. Sci. Technol.*, 2012, **46**(20), 11171–11178.
10 Z. Liu, W. Ye and J. C. Little, Predicting Emissions of Volatile and Semivolatile Organic Compounds from Building Materials: A Review, *Build. Environ.*, 2013, **64**, 7–25.
11 A. M. Calafat, L. Valentin-Blasini and X. Ye, Trends in exposure to chemicals in personal care and consumer products, *Curr. Environ. Health Rep.*, 2015, **2**(4), 348–355.
12 R. E. Dodson, M. Nishioka, L. J. Standley, L. J. Perovich, J. Green Brody and R. A. Rudel, Endocrine Disruptors and Asthma-Associated Chemicals in Consumer Products, *Environ. Health Perspect.*, 2012, **120**(7), 935–943.
13 Y. Guo and K. Kannan, A Survey of Phthalates and Parabens in Personal Care Products from the United States and Its Implications for Human Exposure, *Environ. Sci. Technol.*, 2013, **47**(24), 14442–14449.
14 C. M. A. Eichler, E. A. Cohen Hubal and J. C. Little, Assessing Human Exposure to Chemicals in Materials, Products and Articles: The International Risk Management Landscape for Phthalates, *Environ. Sci. Technol.*, 2019, **53**(23), 13583–13597.
15 H.-M. Shin, T. E. McKone and D. H. Bennett, Model framework for integrating multiple exposure pathways to chemicals in household cleaning products, *Indoor Air*, 2017, **27**, 829–839.
16 L. Huang, A. S. Ernstoff, P. Fantke, S. A. Csiszar and O. Jolliet, A review of models for near-field exposure pathways of chemicals in consumer products, *Sci. Total Environ.*, 2017, **574**, 1182–1208.
17 T. Salthammer, Y. Zhang, J. Mo, H. M. Koch and C. J. Weschler, Assessing human exposure to organic pollutants in the indoor environment, *Angew. Chem., Int. Ed.*, 2018, **57**(38), 12228–12263.
18 C. J. Weschler and W. W. Nazaroff, SVOC partitioning between the gas phase and settled dust indoors, *Atmos. Environ.*, 2010, **44**(30), 3609–3620.

19 G. Bekö, C. J. Weschler, S. Langer, M. Callesen, J. Toftum and G. Clausen, Children's Phthalate Intakes and Resultant Cumulative Exposures Estimated from Urine Compared with Estimates from Dust Ingestion, Inhalation and Dermal Absorption in Their Homes and Daycare Centers, *PLoS One*, 2013, **8**(4), e62442.

20 C. Christia, G. Poma, S. Harrad, C. A. de Wit, Y. Sjostrom, P. Leonards, M. Lamoree and A. Covaci, Occurrence of legacy and alternative plasticizers in indoor dust from various EU countries and implications for human exposure via dust ingestion and dermal absorption, *Environ. Res.*, 2019, **171**, 204–212.

21 D. Kashyap and T. Agarwal, Concentration and factors affecting the distribution of phthalates in the air and dust: A global scenario, *Sci. Total Environ.*, 2018, **635**, 817–827.

22 C. Huang, Y.-J. Zhang, L.-Y. Liu and Y. Guo, Exposure to phthalates and correlations with phthalates in dust and air in South China homes, *Sci. Total Environ.*, 2021, **782**(146806), 1–8.

23 R. Nagorka, W. Birmili, J. Schulze and J. Koschorreck, Diverging trends of plasticizers (phthalates and non-phthalates) in indoor and freshwater environments—why?, *Environ. Sci. Eur.*, 2022, **34**(46), 1–15.

24 C. J. Weschler, T. Salthammer and H. Fromme, Partitioning of phthalates among the gas phase, airborne particles and settled dust in indoor environments, *Atmos. Environ.*, 2008, **42**, 1449–1460.

25 G. C. Morrison, H. Li, S. Mishra and M. Buechlein, Airborne phthalate partitioning to cotton clothing, *Atmos. Environ.*, 2015, **115**, 149–152.

26 *RIVM The DustEx modelling tool*, **https://www.rivm.nl/en/consumer-exposure-to-chemical-substances/exposure-models/dustex**, 2021, accessed January 2023.

27 M. Bakker, C. Delmaar, A. Gerecke, V. Sukiene and N. von Goetz, *Final Report: CEFIC-LRI Project DustEx - Assessing the Relevance of the Dust Contribution in Consumer Exposure to Substances from Consumer Products and Articles (DustEx)*, 2016, p. 152.

28 Y. Xu and J. C. Little, Predicting emissions of SVOCs from polymeric materials and their interaction with airborne particles, *Environ. Sci. Technol.*, 2006, **40**(2), 456–461.

29 C. J. Weschler and W. W. Nazaroff, SVOC exposure indoors: fresh look at dermal pathways, *Indoor Air*, 2012, **22**(5), 356–377.

30 Y. Xu, E. A. Cohen Hubal, P. A. Clausen and J. C. Little, Predicting Residential Exposure to Phthalate Plasticizer Emitted from Vinyl Flooring: A Mechanistic Analysis, *Environ. Sci. Technol.*, 2009, **43**(7), 2374–2380.

31 Y. Liang and Y. Xu, Improved method for measuring and characterizing phthalate emissions from building materials and its application to exposure assessment, *Environ. Sci. Technol.*, 2014, **48**(8), 4475–4484.

32 Y. Liang, X. Liu and M. R. Allen, Measurements of Parameters Controlling the Emissions of Organophosphate Flame Retardants in Indoor Environments, *Environ. Sci. Technol.*, 2018, **52**(10), 5821–5829.

33 Y. Xu, Z. Liu, J. Park, P. A. Clausen, J. L. Benning and J. C. Little, Measuring and Predicting the Emission Rate of Phthalate Plasticizer from Vinyl Flooring in a Specially-Designed Chamber, *Environ. Sci. Technol.*, 2012, **46**(22), 12534–12541.

34 Y. Wu, C. M. A. Eichler, W. Leng, S. S. Cox, L. C. Marr and J. C. Little, Adsorption of Phthalates on Impervious Indoor Surfaces, *Environ. Sci. Technol.*, 2017, **51**(5), 2907–2913.

35 Y. Wu, C. M. A. Eichler, J. Cao, J. L. Benning, A. Olson, S. Chen, C. Liu, E. P. Vejerano, L. C. Marr and J. C. Little, Particle/gas partitioning of phthalates to organic and inorganic airborne particles in the indoor environment, *Environ. Sci. Technol.*, 2018, **52**(6), 3583–3590.

36 J. L. Benning, Z. Liu, A. Tiwari, J. C. Little and L. C. Marr, Characterizing Gas-Particle Interactions of Phthalate Plasticizer Emitted from Vinyl Flooring, *Environ. Sci. Technol.*, 2013, **47**(6), 2696–2703.

37 C. Liu, Y. Zhang, J. L. Benning and J. C. Little, The effect of ventilation on indoor exposure to semivolatile organic compounds, *Indoor Air*, 2015, **25**(3), 285–296.

38 Y. Liang, X. Liu and M. R. Allen, The influence of temperature on the emissions of organophosphate ester flame retardants from polyisocyanurate foam: Measurement and modeling, *Chemosphere*, 2019, **233**, 347–354.

39 Y. Liang and Y. Xu, Emission of Phthalates and Phthalate Alternatives from Vinyl Flooring and Crib Mattress Covers: The Influence of Temperature, *Environ. Sci. Technol.*, 2014, **48**(24), 14228–14237.

40 Y. Liang and Y. Xu, The influence of surface sorption and air flow rate on phthalate emissions from vinyl flooring: Measurement and modeling, *Atmos. Environ.*, 2015, **103**, 147–155.

41 C. M. A. Eichler, Y. Wu, J. Cao, S. Shi and J. C. Little, Equilibrium relationship between SVOCs in PVC products and the air in contact with the product, *Environ. Sci. Technol.*, 2018, **52**(5), 2918–2925.

42 C. K. Addington, K. A. Phillips and K. K. Isaacs, Estimation of the Emission Characteristics of SVOCs from Household Articles Using Group Contribution Methods, *Environ. Sci. Technol.*, 2020, **54**, 110–119.

43 C. J. Weschler and W. W. Nazaroff, Growth of organic films on indoor surfaces, *Indoor Air*, 2017, **27**(6), 1101–1112.

44 C. M. A. Eichler, C. Bi, C. Wang and J. C. Little, A modular mechanistic framework for estimating exposure to SVOCs: Next steps for modeling emission and partitioning of plasticizers and PFAS, *J. Exposure Sci. Environ. Epidemiol.*, 2022, **32**, 356–365.

45 Y. Wu, J. Cao, J. C. Little and Y. Xu, Source/Sink Characteristics of SVOCs, in *Handbook of Indoor Air Quality*, ed. Zhang, Y., Hopke, P. K. and Mandin, C., Springer Nature, Singapore, 2022, pp. 695–740.

46 C. Bi, Y. Liang and Y. Xu, Fate and Transport of Phthalates in Indoor Environments and the Influence of Temperature: A Case Study in a Test House, *Environ. Sci. Technol.*, 2015, **49**(16), 9674–9681.

47 X. Zhang, M. L. Diamond, M. Robson and S. Harrad, Sources, Emissions, and Fate of Polybrominated Diphenyl Ethers and Polychlorinated Biphenyls Indoors in Toronto, Canada, *Environ. Sci. Technol.*, 2011, **45**(8), 3268–3274.

48 Y. Liang and Y. Xu, Improved method for measuring and characterizing phthalate emissions from building materials and its application to exposure assessment, *Environ. Sci. Technol.*, 2014, **48**(8), 4475–4484.

49 J. Cao, X. Zhang, J. C. Little and Y. Zhang, A SPME-based method for rapidly and accurately measuring the characteristic parameter for DEHP emitted from PVC floorings, *Indoor Air*, 2017, **27**(2), 417–426.

50 Y. Wu, S. S. Cox, Y. Xu, Y. Liang, D. Won, X. Liu, P. A. Clausen, L. Rosell, J. L. Benning, Y. Zhang and J. C. Little, A reference method for measuring emissions of SVOCs in small chambers, *Build. Environ.*, 2016, **95**, 126–132.

51 Y. Xu, H. Li and C. Bi, in *A Novel Rapid Method for Characterizing Emissions of Semivolatile Organic Compounds from Building Materials and Consumer Products*, Healthy Buildings Asia; International Society of Indoor Air Quality and Climate, Changsha, China, 2019.

52 Y. Wu, M. Xie, S. S. Cox, L. C. Marr and J. C. Little, Simple method to measure the gas-phase SVOC concentration adjacent to a material surface, *Indoor Air*, 2015, **26**(6), 903–912.

53 M. Xie, Y. Wu, J. C. Little and L. C. Marr, Phthalates and alternative plasticizers and potential for contact exposure from children's backpacks and toys, *J. Exposure Sci. Environ. Epidemiol.*, 2016, **26**, 119–124.

54 A. Manuja, J. Ritchie, K. Buch, Y. Wu, C. M. A. Eichler, J. C. Little and L. C. Marr, Total surface area in indoor environments, *Environ. Sci.: Processes Impacts*, 2019, **21**, 1384–1392.

55 P. A. Clausen, Z. Liu, V. Kofoed-Sorensen, J. Little and P. Wolkoff, Influence of temperature on the emission of Di-(2-ethylhexyl)phthalate (DEHP) from PVC flooring in the emission cell FLEC, *Environ. Sci. Technol.*, 2012, **46**(2), 909–915.

56 M. Song, C. Chi, M. Guo, X. Wang, L. Cheng and X. Y. Shen, Pollution levels and characteristics of phthalate esters in indoor air of offices, *J. Environ. Sci.*, 2015, **28**, 157–162.

57 J. Cao, C. J. Weschler, J. Luo and Y. Zhang, Cm-History Method, a Novel Approach to Simultaneously Measure Source and Sink Parameters Important for Estimating Indoor Exposures to Phthalates, *Environ. Sci. Technol.*, 2016, **50**(2), 825–834.

58 W. Nazaroff, Residential air-change rates: A critical review, *Indoor Air*, 2021, **31**(2), 282–313.

59 S. C. Hammel, J. L. Levasseur, K. Hoffman, A. L. Phillips, A. M. Lorenzo, A. M. Calafat, T. F. Webster and H. M. Stapleton, Children's exposure to phthalates and non-phthalate plasticizers in the home: The TESIE study, *Environ. Int.*, 2019, **132**(105061), 1–10.

60 B. Tang, C. Christia, G. Malarvannan, Y.-E. Liu, X.-J. Luo, A. Covaci, B.-X. Mai and G. Poma, Legacy and emerging organophosphorus flame retardants and plasticizers in indoor microenvironments from Guangzhou, South China, *Environ. Int.*, 2020, **143**(105972), 1–15.

61 J. Huang, X. Wang, J.-Q. Guo, X. Wang, M. Ji and L. Huang, Partition of phthalates among air, PM2.5, house dust and skin in residential indoor environments, *Indoor Air*, 2022, **32**(11), e13176.

62 EFSA, Update of the risk assessment of di-butylphthalate (DBP), butyl-benzyl-phthalate (BBP), bis(2-ethylhexyl) phthalate (DEHP), di-isononylphthalate (DINP) and di-isodecylphthalate (DIDP) for use in food contact materials, *EFSA J.*, 2019, **17**(12), e05838.

63 ATSDR Minimal Risk Levels (MRLs) for Hazardous Substances, **https://wwwn.cdc.gov/TSP/MRLS/mrlslisting.aspx**, 2021, accessed Feb 8, 2023.

64 Y. Wu, Z. Song, J. C. Little, M. Zhong, H. Li and Y. Xu, An integrated exposure and pharmacokinetic modeling framework for assessing population-scale risks of phthalates and their substitutes, *Environ. Int.*, 2021, **156**, 106748.